Paleoceanography and Paleoclimatology

RESEARCH ARTICLE
10.1029/2024PA005043

Early Pliocene Shoaling of the Central American Seaway Reconstructed From Foraminifera-Bound Nitrogen and Oxygen Isotopes

Jesse R. Farmer[1,2,3], Alfredo Martínez-García[2], Lori T. Sentman[4], Ralf Schiebel[2], Anthea Arns[2], Maayan Yehudai[2], Ralf Tiedemann[5], Daniel M. Sigman[3], and Gerald H. Haug[2,6]

[1]School for the Environment, University of Massachusetts Boston, Boston, MA, USA, [2]Climate Geochemistry, Max-Planck Institute for Chemistry, Mainz, Germany, [3]Department of Geosciences, Princeton University, Princeton, NJ, USA, [4]National Oceanic and Atmospheric Administration, Office of Oceanic and Atmospheric Research, Geophysical Fluid Dynamics Laboratory (GFDL), Princeton, NJ, USA, [5]Alfred Wegener Institute, Bremerhaven, Germany, [6]Department of Earth Sciences, ETH Zürich, Zurich, Switzerland

Key Points:

- Foraminifera-bound nitrogen isotopes trace the early Pliocene restriction of nutrient exchange across the Central American Seaway
- Geochemical data indicate four phases of seaway shoaling between 4.6 and 4.1 million years ago
- Climatically relevant oceanic exchanges across the Central American Seaway ended after 4.1 million years ago

Correspondence to:
J. R. Farmer,
jesse.farmer@umb.edu

Citation:
Farmer, J. R., Martínez-García, A., Sentman, L. T., Schiebel, R., Arns, A., Yehudai, M., et al. (2025). Early Pliocene shoaling of the Central American Seaway reconstructed from foraminifera-bound nitrogen and oxygen isotopes. *Paleoceanography and Paleoclimatology*, *40*, e2024PA005043. https://doi.org/10.1029/2024PA005043

Received 17 OCT 2024
Accepted 7 APR 2025

Author Contributions:
Conceptualization: Jesse R. Farmer, Alfredo Martínez-García, Ralf Schiebel, Daniel M. Sigman, Gerald H. Haug
Formal analysis: Jesse R. Farmer, Lori T. Sentman, Anthea Arns, Maayan Yehudai
Funding acquisition: Alfredo Martínez-García, Daniel M. Sigman, Gerald H. Haug
Investigation: Jesse R. Farmer, Lori T. Sentman, Anthea Arns, Maayan Yehudai
Methodology: Jesse R. Farmer, Alfredo Martínez-García, Ralf Schiebel, Ralf Tiedemann, Daniel M. Sigman
Project administration: Jesse R. Farmer, Alfredo Martínez-García, Ralf Schiebel, Daniel M. Sigman, Gerald H. Haug
Resources: Alfredo Martínez-García, Ralf Tiedemann
Software: Lori T. Sentman

Abstract The formation of the Isthmus of Panama closed the Central American Seaway, severing the only Late Cenozoic low-latitude connection between the Pacific and Atlantic Oceans. Here we clarify the Early Pliocene (5.3–3.6 million years ago [Ma]) sequence of events associated with the shoaling of the Central American Seaway based on differences in upper ocean biogeochemical properties between the eastern tropical North Pacific (ETNP) and the Caribbean Sea. Foraminifera-bound nitrogen isotopes (FB-δ^{15}N) are elevated in the ETNP relative to the Caribbean Sea throughout the Early Pliocene. Whereas ETNP FB-δ^{15}N shows no long-term trend across the Early Pliocene, FB-δ^{15}N in the Caribbean Sea declines by ∼0.5‰ between 4.6 and 4.5 Ma, and by an additional ∼1‰ between 4.35 and 4.25 Ma. We interpret the divergence between ETNP and Caribbean Sea FB-δ^{15}N to indicate progressive isolation of their subsurface nutrient pools due to CAS shoaling. The oxygen isotopic composition of seawater ($\delta^{18}O_{sw}$) derived from planktonic foraminifer δ^{18}O and Mg/Ca shows a small but variable gradient between the ETNP and Caribbean Sea over the Early Pliocene, with a trend toward a larger $\delta^{18}O_{sw}$ gradient after 4.25 Ma. We suggest that the development of persistent chemical differences in both thermocline nutrients and surface waters between the ETNP and Caribbean Sea after 4.1 Ma reflects the cessation of basin-scale oceanic exchanges across the Central American Seaway.

Plain Language Summary The Central American Seaway was the last tropical connection between the Atlantic and Pacific Oceans in Earth's history. Despite numerous studies, the timing and sequence of events leading to the closure of the seaway remain debated. Here we present new chemical data measured in marine sediments that speak to the transport of seawater and associated nutrients across the seaway. Our results focus on a time when existing data indicate a critical shoaling of the seaway. By comparing our chemical results with a computer simulation of ocean transport, we find four phases of progressive shallowing of the seaway between 4.6 and 4.1 million years ago. Our chemical data indicate limited exchange between the Pacific and Atlantic Oceans after 4.1 million years ago. We interpret this to indicate that the seaway was effectively closed at an oceanic scale after 4.1 million years ago, although our results do not rule out the existence of small, shallow passageways in the Panama Isthmus into the late Pliocene.

1. Introduction

The closure of the Central American Seaway (CAS) via the formation of the Panama Isthmus and the linking of North and South America is one of the best studied and most vigorously debated tectonic events of the Neogene. Published dates of CAS closure based on geological, geochemical, and biological inferences from the stratigraphic record span over 20 million years, from the early Miocene ca. 23 million years ago (Ma) (Bacon et al., 2015) to the late Pliocene ca. 2.5 Ma (Groeneveld et al., 2014). This chronological uncertainty arises from the complex geological setting of the Panama Isthmus, as well as the varied sources of information (geologic, geochemical, molecular, and paleontological) that recorded aspects of CAS closure (e.g., Saito, 1976; Keigwin, 1982; Haug et al., 2001; Coates et al., 2004; Lessios, 2008; Montes et al., 2015; McGirr et al., 2021; Vallejo-Hincapié et al., 2024; summarized in Bacon et al., 2015; O'Dea et al., 2016). However, uncertainty on the timing of CAS closure challenges interpretations of how this event related to Neogene climate evolution. For instance,

Supervision: Alfredo Martínez-García, Ralf Schiebel, Daniel M. Sigman, Gerald H. Haug
Visualization: Jesse R. Farmer
Writing – original draft: Jesse R. Farmer, Alfredo Martínez-García, Lori T. Sentman, Anthea Arns, Ralf Tiedemann, Daniel M. Sigman, Gerald H. Haug
Writing – review & editing: Jesse R. Farmer, Alfredo Martínez-García, Lori T. Sentman, Anthea Arns, Maayan Yehudai, Ralf Tiedemann, Daniel M. Sigman, Gerald H. Haug

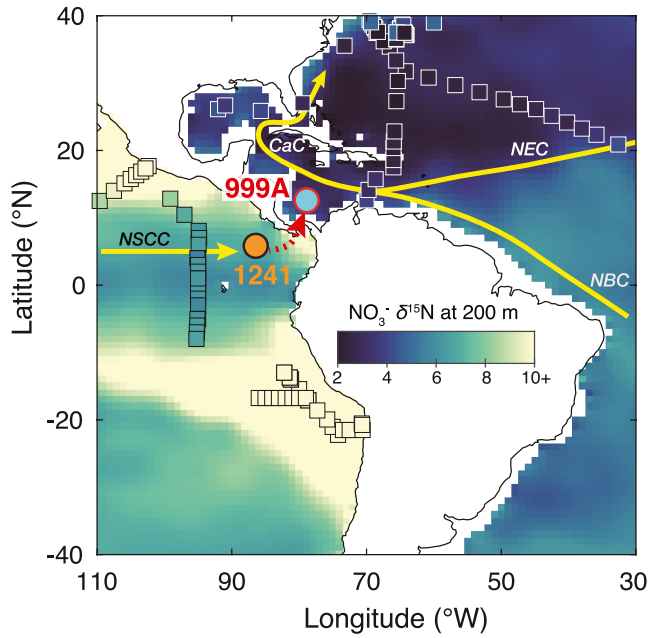

Figure 1. Study locations, modern-day hydrography and δ^{15}N of nitrate in the thermocline. Squares indicate locations and δ^{15}N of nitrate measured between 150 and 250 m depth (compiled by Fripiat et al., 2021). Gridded field is predicted nitrate δ^{15}N at 200 m depth from an artificial neural network ensemble (Rafter et al., 2019). Site 999 Hole A (red outlined cyan circle) in the Caribbean Sea receives low-δ^{15}N thermocline nitrate advected from the tropical Atlantic via the North Equatorial Current (NEC) and North Brazil Current (NBC). Site 1241 (black outlined orange circle) in the eastern tropical Pacific receives thermocline nitrate from the Northern Subsurface Counter Current (NSCC).

CAS closure has alternatively been considered a proximal cause of the late Pliocene intensification of Northern Hemisphere glaciation (INHG, ~2.7 Ma) (Keigwin, 1982), a necessary precondition for the INHG (Haug et al., 2001; Haug & Tiedemann, 1998; Lear et al., 2003), or a consequence of changes to Earth's climate system (e.g., lowered global sea level) during the Pliocene that were separate from the INHG (Lunt et al., 2008; Molnar, 2008).

Deep sea sediments in the Caribbean Sea and eastern tropical Pacific Ocean provide continuous records across the time intervals considered to encompass CAS shoaling (Figure 1). Proxy measurements, most notably the oxygen isotopic composition of mixed layer-dwelling planktonic foraminifera ($\delta^{18}O_{pf}$), have indicated divergence of Caribbean and Pacific surface water salinities in the Pliocene Epoch (5.33–2.6 million years ago [Ma]) due to restricted oceanic exchange across a shoaled and/or closed CAS (Haug et al., 2001; Keigwin, 1982; Steph, Tiedemann, Prange, et al., 2006). However, the interpretation of $\delta^{18}O_{pf}$ in terms of salinity is challenged by the confounding influence of temperature on $\delta^{18}O_{pf}$ and the potential for drivers of salinity gradients between the Caribbean and Pacific unrelated to CAS shoaling, such as river re-routing from Andean mountain uplift and/or migration of the intertropical convergence zone (e.g., Molnar, 2008; Steph, Tiedemann, Prange, et al., 2006).

The nitrogen isotopic composition (expressed in δ notation as δ^{15}N) of nitrate within the shallow subsurface ocean varies by ~20 parts per thousand (‰), in part due to intra- and inter-basin gradients in fixed nitrogen sources (most importantly, N_2 fixation) and sinks (water column and sedimentary denitrification) (e.g., Casciotti, 2016; Farmer, Fehrenbacher, et al., 2025). Recent studies have utilized FB-δ^{15}N to trace past geological constraints on subsurface ocean nitrate transport across ocean gateways (Farmer et al., 2021, 2023). Here we apply this approach to the early Pliocene (5.3–3.6 Ma) shoaling of the CAS using FB-δ^{15}N measurements at Ocean Drilling Program (ODP) Site 999 in the Caribbean Sea and Site 1241 in the Eastern Tropical North Pacific (ETNP). Today, the Isthmus of Panama separates thermocline waters with distinct nitrate δ^{15}N values (Figure 1). The δ^{15}N of thermocline nitrate in the Caribbean and tropical to subtropical North Atlantic (~3‰) is lower than that of the mean ocean due to the regional occurrence of nitrogen fixation (Knapp et al., 2005; Marconi et al., 2017). In contrast, the δ^{15}N of thermocline nitrate in the ETNP is elevated (to ≥7‰; Sigman et al., 2005) due to its proximity to the ETNP oxygen deficient zone (Kwiecinski & Babbin, 2021). In this setting, preferential microbial consumption of

^{14}N-nitrate as a terminal electron acceptor ("denitrification") leaves the residual water column nitrate elevated in δ^{15}N (Cline & Kaplan, 1975).

Prior to the closure of the CAS, it is expected that the thermocline nitrate δ^{15}N gradient between the ETNP and Caribbean Sea would have been reduced. In experiments with an open CAS, box models and ESMs consistently show net eastward (Pacific-to-Atlantic) transport of surface and thermocline waters (e.g., Khon et al., 2023; Sentman et al., 2018; Sepulchre et al., 2014; Steph et al., 2010). If the ETNP hosted water column denitrification and the Caribbean did not during the early Pliocene, an open CAS would have allowed for high-δ^{15}N nitrate to be transported from the ETNP into the Caribbean Sea, thus raising the δ^{15}N of thermocline nitrate within the Caribbean. In turn, once the CAS had sufficiently shoaled to limit subsurface nutrient transport, the supply of high-δ^{15}N nitrate from the ETNP into the Caribbean Sea would have ceased. Thus, our initial expectation is that δ^{15}N of thermocline nitrate in the Caribbean Sea should have declined as CAS shoaling progressed.

Conceptually, the isotopic and elemental composition of the carbonate tests of mixed layer-dwelling planktonic foraminifera is set primarily by the seawater properties of their calcification environment (in this case, the mixed layer). In contrast, the nitrogen isotopic composition of the shell-bound organic matter of mixed-layer dwelling planktonic foraminifera principally sources from the nitrate supply beneath the mixed layer. This is because the supply of subsurface nitrate to the euphotic zone sustains new production (Eppley & Peterson, 1979), and this new production in turn provides nitrogen to planktonic foraminifera through their diet. This simple framework is supported by the observed correlation between the δ^{15}N of mixed-layer dwelling planktonic foraminifera-bound organic matter (FB-δ^{15}N) and the δ^{15}N of nitrate within the underlying shallow subsurface ocean in nitrate-limited oligotrophic environments (Ren et al., 2012; Schiebel et al., 2018; Smart et al., 2018), such as occurs above Sites 999 and 1241 today.

In this study, we revisit the Early Pliocene history of CAS shoaling using a combination of FB-δ^{15}N as a tracer of thermocline nitrate exchange across the CAS and an updated reconstruction of surface (mixed layer) connectivity by comparing the oxygen isotopic composition of seawater ($\delta^{18}O_{sw}$), a correlate of salinity, derived from existing $\delta^{18}O_{pf}$ data (Haug et al., 2001; Steph, Tiedemann, Prange, et al., 2006) and mixed layer temperature reconstructions from magnesium-to-calcium ratios (Mg/Ca) in planktonic foraminifera (Groeneveld, 2005; Groeneveld et al., 2006; O'Brien et al., 2014). The interpretive framework for using thermocline nitrogen and mixed layer oxygen isotope gradients as indicators of CAS shoaling is informed from open/shoaled/closed CAS sensitivity experiments (Sentman et al., 2018) performed with the fully coupled Geophysical Fluid Dynamics Laboratory (GFDL) Earth System Model (ESM), GFDL-ESM2G (Dunne et al., 2012, 2013).

2. Materials and Methods

2.1. Sediment Samples and Nitrogen Isotope Analyses

ODP Sites 999 Hole A (12.7°N, 78.7°W, 2,838 m water depth) and 1241 (5.8°N, 86.4°W, 2,027 m water depth) were sampled at 20–40 cm resolution between 5.3 and 3.6 Ma. The age model for Site 999 was previously established by tuning benthic δ^{18}O to the LR04 benthic δ^{18}O stack (Lisiecki & Raymo, 2005; see details in Öğretmen et al., 2020). The age model for Site 1241 was previously established by tuning physical properties and benthic δ^{13}C to orbital parameters, and is confirmed by the alignment of Site 1241 benthic δ^{18}O to the LR04 benthic stack (Tiedemann et al., 2007).

Two to three hundred specimens of the mixed layer-dwelling, dinoflagellate symbiont-bearing planktonic foraminifer *Trilobatus sacculifer* (formerly *Globigerinoides sacculifer*; Spezzaferri et al., 2015) were picked from the >250 μm size fraction of Sites 999 and 1241. Where *T. sacculifer* was relatively rare at Site 1241, one hundred specimens of the abundant, shallow subsurface-dwelling and symbiont-barren planktonic foraminifer *Globorotalia menardii* and its sister taxa *Globortalia tumida* were picked. FB-δ^{15}N was measured using the persulfate-denitrifier technique at Max Planck Institute for Chemistry following existing protocols for carbonate cleaning (Farmer et al., 2021), oxidation of bound organic nitrogen to nitrate (Knapp et al., 2005), conversion of nitrate to N_2O via denitrifying bacteria (Sigman et al., 2001), and measurement of N isotopes on N_2O using a purpose-built purge and trap system connected to a Thermo MAT253 Plus mass spectrometer (Martínez-García et al., 2022; Weigand et al., 2016). Analytical precision (±1sd) was evaluated using the long-term precision of in-house carbonate standards (≤0.30‰, Moretti et al., 2024) and full procedural replicate analyses of foraminifera samples (±0.16‰, n = 32 for Site 999; ±0.18‰, n = 39 for Site 1241).

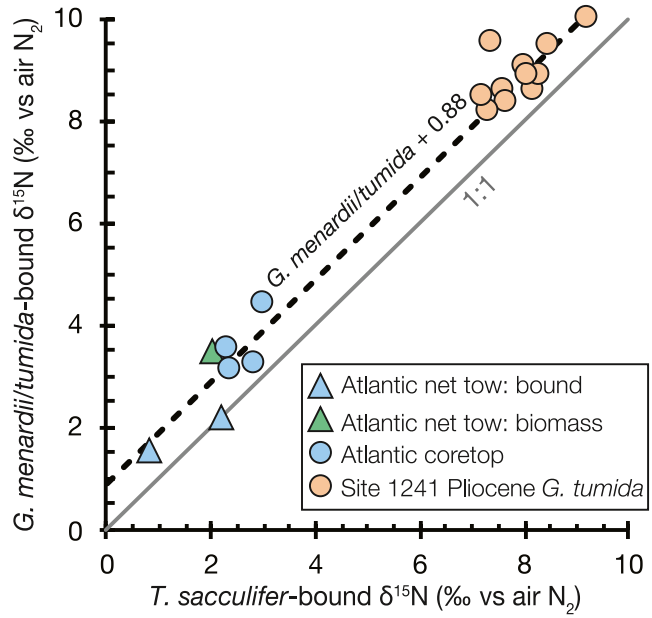

Figure 2. Comparison of *T. sacculifer* and *G. menardii/G. tumida*-bound δ^{15}N. Shown are foraminifer biomass collected during a new tow in the subtropical North Atlantic (green diamond; Ren et al., 2012), foraminifer-bound organic matter δ^{15}N (FB-δ^{15}N) collected during net tows in the subtropical North Atlantic (blue triangles; Smart et al., 2018), coretop FB-δ^{15}N from the north and tropical Atlantic (blue circles; Ren et al., 2012), and downcore FB-δ^{15}N measurements from Site 1241 where *T. sacculifer* and *G. menardii* were measured in the same sediment depth (orange circles). All available data are well described by a positive offset in *G. menardii/G. tumida* FB-δ^{15}N of 0.88‰ relative to *T. sacculifer* FB-δ^{15}N (dashed line).

No significant difference has been observed between FB-δ^{15}N in *G. menardii* and *G. tumida* in samples where both taxa co-occur (M. Lacerra, pers. comm.). In 11 samples where FB-δ^{15}N was measured in both *G. menardii/G. tumida* and *T. sacculifer*, the FB-δ^{15}N of *G. menardii/G. tumida* was 0.88 ± 0.24‰ (1sd) higher than in *T. sacculifer* (Figure 2). This FB-δ^{15}N difference between taxa is consistent with measurements of modern foraminifer biomass δ^{15}N and FB-δ^{15}N in net tows, and FB-δ^{15}N in coretops, of *G. menardii* and *T. sacculifer* in the subtropical Atlantic Ocean (average δ^{15}N elevation in *G. menardii* biomass of 0.85 ± 0.54‰ relative to *T. sacculifer*; Ren et al., 2012; Smart et al., 2018) (Figure 2). Thus, we applied a constant −0.88‰ correction to *G. menardii/tumida* FB-δ^{15}N and present them as *T. sacculifer*-equivalent FB-δ^{15}N values throughout.

2.2. Calculation of Seawater δ^{18}O

The oxygen isotopic composition of seawater ($\delta^{18}O_{sw}$) was calculated using PSU Solver (Thirumalai et al., 2016) from existing δ^{18}O and Mg/Ca measurements on *T. sacculifer* at Sites 999 and 1241 (Groeneveld, 2005; Groeneveld et al., 2006; Haug et al., 2001; Steph, Tiedemann, Prange, et al., 2006). Mg/Ca values were converted to sea surface temperature (SST) using the calibration of Dekens et al. (2002) with depth correction and assuming constant modern seawater Mg/Ca. Local $\delta^{18}O_{sw}$ was calculated from salinity using the tropical Atlantic (for Site 999) and tropical Pacific (for Site 1241) relationships (LeGrande & Schmidt, 2006). We note that, as our focus is on the $\delta^{18}O_{sw}$ gradient between two sites, the exact choice of Mg/Ca to SST calibration (Gray & Evans, 2019) or inclusion of a secular seawater Mg/Ca change (O'Brien et al., 2014) would not alter our results because the Site 999 and 1241 records are affected similarly. Probabilistic 1 standard deviation (1sd)-equivalent (68%) uncertainties on reconstructed $\delta^{18}O_{sw}$ from PSU Solver were ±0.21‰ at Site 999 and ±0.15‰ at Site 1241. The probabilistic 1sd-equivalent uncertainty on the $\delta^{18}O_{sw}$ gradient between Sites 999 and 1241 was determined by addition of the site-specific uncertainties in quadrature, and averages ±0.25‰.

To visualize longer-term trends unrelated to low latitude orbital forcing (19–23 kyr precession and 41 kyr obliquity), 100 kyr lowpass filters were calculated for each data series in Matlab R2021a using hepta_smooth.m (Emile-Geay, 2015).

2.3. Modeling of CAS Transport

To characterize how CAS shoaling would affected subsurface nutrients and surface mixed layer $\delta^{18}O_{sw}$ in the Caribbean Sea, we employ sensitivity simulations of ocean volume transport across the CAS using GFDL-ESM2G (Sentman et al., 2018). GFDL-ESM2G is a fully coupled Earth system model and includes an interactive ocean biogeochemical component, TOPAZ2 (Dunne et al., 2012, 2013). GFDL-ESM2G bathymetry was configured for two idealized open CAS simulations, *Wide* (2,000 km long, 2,000 m deep CAS), *WideShallow* (2,000 km long, 200 m deep CAS), and a third *Closed* simulation (preindustrial control) (Sentman et al., 2018) (Figure 3). Note that the simulations are not intended to accurately reproduce the complex geologic history of the CAS or Panama Isthmus (e.g., Coates et al., 2004; McGirr et al., 2021; Montes et al., 2012, 2015; Vallejo-Hincapié et al., 2024). Instead, these simulations only differ in their CAS bathymetry and provide a controlled experiment testing how oceanic transport would change across the CAS strictly in response to shoaling. The experiments were initialized from a preindustrial (year 1860) climate state established with modern ocean temperature, salinity, nitrate, phosphate, silicate and oxygen from World Ocean Atlas 2005 (Antonov et al., 2006; Garcia et al., 2006a, Garcia et al., 2006b; Locarnini et al., 2006) and alkalinity and preindustrial dissolved inorganic carbon from GLODAP (Key et al., 2004) (see details in Dunne et al., 2013).

Ocean transports originally calculated within a broad domain (4°–18°N, 260° to 283°E) by Sentman et al. (2018) were updated here by restricting the domain to model grid points that are currently above sea level (Figures 3a and 3b). Modern vertical profiles of nitrate concentration and salinity observed at the locations of Sites 999 and 1241 are shown compared to simulated profiles using GFDL-ESM2G in Figure 3. Model-based $\delta^{18}O_{sw}$ was interpreted from simulated salinity using the modern $\delta^{18}O_{sw}$-salinity relationships (Section 2.2).

2.4. CAS Shoaling and Pliocene Mixed Layer Depth

Interpreting FB-$\delta^{15}N$ in terms of past shallow subsurface nitrate exchange across the CAS requires constraints on the depth of the nitrate-poor mixed layer, as nitrate transport between the ETNP and Caribbean would only occur below this depth. We note that changes in mixed layer depth alone should not affect FB-$\delta^{15}N$ because nitrate $\delta^{15}N$ is effectively homogenous between the thermocline and approximately 300 m depth in both the Caribbean Sea and ETNP (e.g., Rafter et al., 2012). Thus, both shallower and deeper mixed layers would be expected to entrain subsurface nitrate of the same $\delta^{15}N$. Instead, changes in the mixed layer depth would affect our interpretation of the depth to which the CAS would need to shoal in order to restrict subsurface nitrate transport.

Today, the Caribbean Sea at Site 999 is characterized by a ∼22–70 m deep mixed layer, deeper than the ∼10–30 m deep mixed layer in the ETNP overlying Site 1241 (Holte et al., 2017). In the early Pliocene, $\delta^{18}O$ and Mg/Ca measurements in shallow subsurface-dwelling foraminifera (*G. tumida*) indicate warmer conditions at ∼100 m depth compared to today, which could result from a deepening of the mixed layer and/or a warming of thermocline waters during the Pliocene (Steph, Tiedemann, Groeneveld, et al., 2006, 2010; Ford et al., 2012, 2015). However, maintained high productivity in the eastern equatorial Pacific throughout the Piocene argues against significant mixed-layer deepening at this time (Dekens et al., 2007). In GFDL-ESM2G, the mixed layer depth overlying Site 1241 maintains as ∼30 m in all three modeled scenarios (Figures 3c and 3d), also contradicting a deeper mixed layer during the Pliocene. Given the above, we conservatively estimate that the ETNP mixed layer overlying Site 1241 did not exceed 50 m depth in the Early Pliocene, such that any transport of ETNP waters shallower than 50 m across the CAS would be nitrate-poor and would not influence Caribbean Sea FB-$\delta^{15}N$.

3. Results

3.1. Oxygen and Nitrogen Isotopes

Proxies indicative of surface mixed layer conditions (*T. sacculifer* $\delta^{18}O$, Mg/Ca, and calculated $\delta^{18}O_{sw}$) at Sites 999 and 1241 are shown in Figure 4. Site 1241 and Site 999 $\delta^{18}O_{pf}$ values are similar from 5.3 until ∼4.2 Ma, after which Site 999 $\delta^{18}O_{pf}$ increases (Figure 4b), signaling the emergence of a Pacific-Caribbean $\delta^{18}O_{pf}$ gradient as previously observed (Haug et al., 2001; Keigwin, 1982; Steph, Tiedemann, Prange, et al., 2006). Whether this $\delta^{18}O_{pf}$ gradient reflects the emergence of a temperature or salinity gradient requires additional constraints on temperature at each location. *T. sacculifer* Mg/Ca differs between Sites 999 and 1241 (Figure 4c), indicating that the Early Pliocene mixed layer thermal histories were different in the ETNP and Caribbean Sea (Groeneveld, 2005; Groeneveld et al., 2006). Specifically, the surface mixed layer was generally warmer in the Caribbean

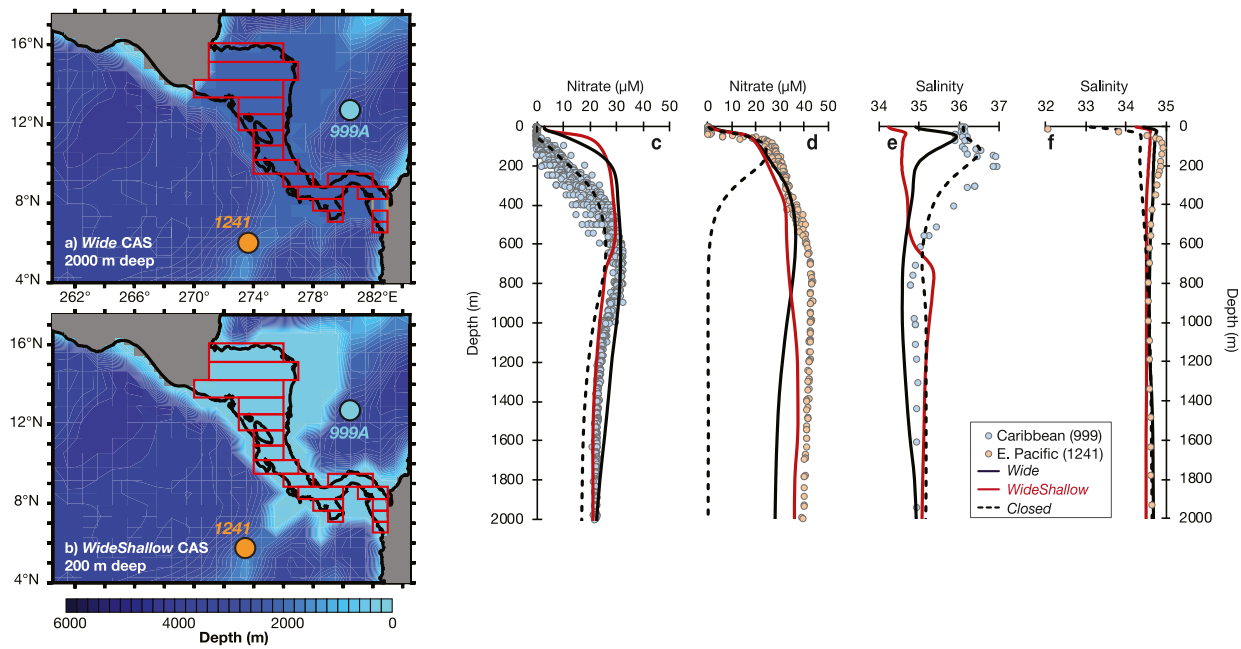

Figure 3. Updated domain for calculation of volume transports and comparison of hydrographic data at Sites 999 and 1241 with GFDL-ESM2G. In (a)–(b), red outlined area denotes model grid points where net west-to-east volume transports were summed; these transports were originally summed across the entire map domain of these panels by Sentman et al. (2018). Seafloor depth in (a) and (b) indicated by the colorbar. Preindustrial control coastlines (black) and land area (gray) in GFDL-ESM2G are shown in both panels for reference. See Sentman et al. (2018) for additional details. Blue and orange circles in, and (c)–(f) are hydrographic data near the locations of Site 999 in the Caribbean Sea and Site 1,241 in the Eastern Tropical North Pacific, respectively (Garcia et al., 2019). Nitrate concentrations are shown in panels c and d; salinity is shown in panels e and f. Black dashed line in each panel is the preindustrial control with a closed CAS; black solid line is the *Wide* experiment; red solid line is the *WideShallow* experiment. Note that GFDL-ESM2G has a known bias toward sluggish tropical ventilation (Dunne et al., 2012, 2013), which leads to an unrealistically large oxygen deficient zone and extreme denitrification (to nitrate depletion) below 400 m in the ETNP from the preindustrial control experiment.

(higher *T. sacculifer* Mg/Ca at Site 999) relative to the ETNP prior to 4.6 Ma, with a transition to a cooler Caribbean surface mixed layer (lower *T. sacculifer* Mg/Ca at Site 999) relative to the ETNP after 4.6 Ma (Groeneveld, 2005; Groeneveld et al., 2006; O'Brien et al., 2014).

Combining *T. sacculifer* $\delta^{18}O_{pf}$ and Mg/Ca-derived mixed layer temperature (Groeneveld et al., 2006; O'Brien et al., 2014), we calculate the change in mixed layer $\delta^{18}O_{sw}$, which strongly correlates with salinity in the modern low latitude ocean (LeGrande & Schmidt, 2006). Site 1241 shows generally constant $\delta^{18}O_{sw}$ values of +0.5‰ throughout the Early Pliocene. Mean $\delta^{18}O_{sw}$ values are not significantly different between 5.3 and 4.2 Ma compared to between 4.2 and 3.6 Ma (two-tailed heteroscedastic *t*-test, $p = 0.86$), suggestive of no long-term salinity change in the ETNP mixed layer at this location between 5.3 and 3.6 Ma (Figure 4d; see also Groeneveld et al., 2006). In contrast, Site 999 $\delta^{18}O_{sw}$ shows greater temporal variation, with similar or slightly elevated values relative to Site 1241 between 5.3 and 4.2 Ma, followed by a significant shift to higher $\delta^{18}O_{sw}$ values after 4.2 Ma (two-tailed heteroscedastic *t*-test, $p = 0.001$). These shifts indicate that the salinity of the Caribbean mixed layer was similar to or only slightly higher than the ETNP prior to 4.2 Ma; a more saline Caribbean mixed layer emerged after 4.2 Ma, and particularly around 4.1 Ma and between 3.9 and 3.7 Ma (Figure 4d).

The FB-$\delta^{15}N$ results tracking thermocline nitrate sources show a related but distinct pattern (Figure 4e). At Site 1241 in the ETNP, FB-$\delta^{15}N$ ranges from 7.1 to 9.5‰, with no significant difference between FB-$\delta^{15}N$ averages from 5.3 to 4.2 Ma (8.1 ± 0.5‰, 1sd) and from 4.2 to 3.6 Ma (8.0 ± 0.5 ‰) (two-tailed heteroscedastic *t*-test, $p = 0.342$). As is the case for $\delta^{18}O_{sw}$, Site 1241 shows no apparent long-term trend in FB-$\delta^{15}N$. Instead, there is ~2‰ of FB-$\delta^{15}N$ variability around the 100 kyr lowpass filtered trend. This variability is similar in magnitude to the obliquity-paced variations in bulk sediment $\delta^{15}N$ at the more northern ODP Site 1012 (Liu et al., 2008) in the eastern subtropical North Pacific (32.3°N, 118.4°W) over the last 4 million years, which are interpreted to reflect changes in the extent and/or intensity of water column denitrification (Figure 5a). However, our sampling resolution at Site 1241 (1 sample per ~15 kyr) is too low to capture obliquity-paced variations. We posit that the FB-$\delta^{15}N$ variability at Site 1241 represents aliasing of obliquity-paced changes in the extent or intensity of water

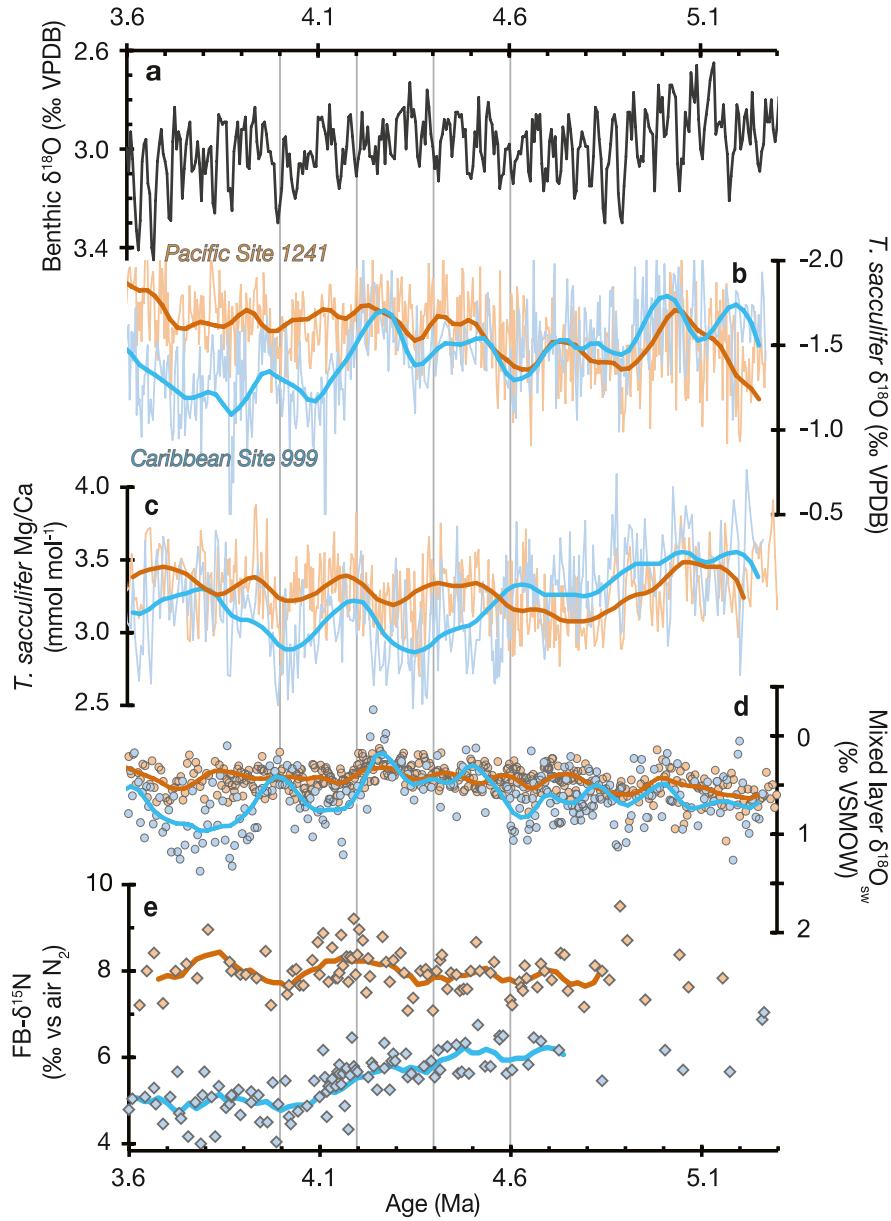

Figure 4. Elemental and isotopic measurements on planktonic foraminifera from Sites 999 and 1241 between 5.3 and 3.6 Ma. (a) Benthic δ^{18}O stack (Lisiecki & Raymo, 2005), (b) *T. sacculifer* δ^{18}O from the eastern tropical Pacific (Site 1241, orange) and Caribbean Sea (Site 999, blue), (c) *T. sacculifer* Mg/Ca, a proxy for mixed layer temperature, (d) Calculated mixed layer $\delta^{18}O_{sw}$ using *T. sacculifer* δ^{18}O (b) and Mg/Ca-derived temperature (c) (Section 2.2), and (e) *T. sacculifer*-bound FB-δ^{15}N. Thick lines in (b)–(e) indicate 100 kyr lowpass filters (Section 2.2). Vertical lines denote 4.6, 4.4, 4.2, and 4.0 Ma.

column denitrification in the ETNP, a hypothesis that can be tested by increasing the resolution of the Site 1241 FB-δ^{15}N record.

In the Caribbean Sea, FB-δ^{15}N at Site 999 ranges from 4.0 to 7.0‰ (Figure 4e), but shows a significant decline in FB-δ^{15}N averages from 5.3 to 4.2 Ma (5.9 ± 0.4‰) and from 4.2 to 3.6 Ma (5.1 ± 0.5‰) (two-tailed heteroscedastic *t*-test, $p < 0.001$). The highest Site 999 FB-δ^{15}N values occur prior to 4.2 Ma, with a pronounced 1‰ FB-δ^{15}N decline between 4.2 and 4.0 Ma, and relatively constant FB-δ^{15}N values after 4.0 Ma. Site 999 FB-δ^{15}N also shows ∼1.5–2‰ of variability around the lowpass filtered trends, which is of similar magnitude to the precession-paced variations in FB-δ^{15}N at Site 999 over the last 160 kyr (Figure 5b; Straub et al., 2013). As at Site 1241, the Pliocene FB-δ^{15}N resolution at Site 999 is too low (1 sample per ∼13 kyr) to capture precession-paced

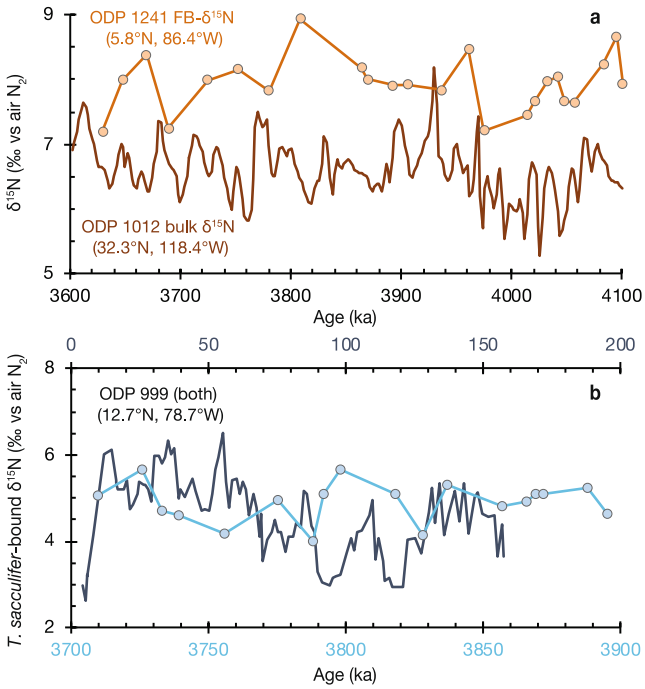

Figure 5. Pliocene FB-δ^{15}N results from (a) Site 1241, and (b) Site 999 with comparison δ^{15}N records. (a) FB-δ^{15}N from Site 1241 (orange circles, this study) with bulk sediment δ^{15}N from ODP Site 1012 (brown line), an indicator of ETNP denitrification (Liu et al., 2008), from 3.6 to 4.1 Ma. ODP 1012 bulk sediment δ^{15}N shows ~2‰ variations at approximately obliquity periodicities (Liu et al., 2008). FB-δ^{15}N from Site 1241 shows a similar magnitude of variation (~2‰) but is not of sufficient resolution to resolve orbital periodicities. (b) *T. sacculifer* FB-δ^{15}N from Site 999 during a 200 kyr Pliocene window of 3.9 to 3.7 Ma (cyan, this study) compared against *T. sacculifer* FB-δ^{15}N from Site 999 over the last 200 ka (dark blue; Straub et al., 2013). The lower resolution Pliocene record (this study) shows a similar range as was observed over the last glacial cycle, with the notable exception of interglacial minima.

variations, and we suggest that the FB-δ^{15}N variability at Site 999 represents aliasing of orbitally driven changes in the intensity of shelf sedimentary denitrification and associated N_2 fixation in the tropical Atlantic (Auderset et al., 2024; Straub et al., 2013). Most important for the current study, the magnitude of FB-δ^{15}N decline at Site 999 between 4.2 and 4.0 Ma did not occur at ETNP Site 1241.

4. Discussion

4.1. Limitations of $\delta^{18}O_{sw}$ as a Tracer of CAS Shoaling

The δ^{18}O of planktonic foraminifera in the Caribbean and East Pacific has long served as a primary indicator of CAS shoaling history (Haug et al., 2001; Keigwin, 1982; O'Dea et al., 2016) largely due to the clear $\delta^{18}O_{pf}$ divergence in the early Pliocene (Figure 4b). This feature would be expected to also appear in $\delta^{18}O_{sw}$ due to the strong correlation of $\delta^{18}O_{sw}$ to salinity and the large salinity gradient across the modern isthmus of Panama (e.g., Haug et al., 2001). While the $\delta^{18}O_{sw}$ records at Site 999 and 1241 do exhibit increasing divergence through the early Pliocene, this divergence is, if anything, muted compared to $\delta^{18}O_{pf}$ (Figure 4d). Absolute $\delta^{18}O_{sw}$ differences between Sites 999 and 1241 do not exceed 1‰; over much of the early Pliocene, there is no statistically significant $\delta^{18}O_{sw}$ difference between the Caribbean and ETNP considering a pooled probabilistic 1sd-equivalent uncertainty of ±0.25‰ on the $\delta^{18}O_{sw}$ gradient (Section 2.2).

As temperature is an input for the deconvolution of $\delta^{18}O_{pf}$ to $\delta^{18}O_{sw}$, the robustness of $\delta^{18}O_{sw}$ reconstructions is contingent upon the robustness of the paleotemperature reconstructions used. One source of the muted $\delta^{18}O_{sw}$ difference between Sites 999 and 1241 compared to their $\delta^{18}O_{pf}$ is out-of-phase changes in reconstructed temperature (from Mg/Ca) and $\delta^{18}O_{pf}$ at Site 999 (compare Figures 4b and 4c). This does not appear to be an underlying issue with the Mg/Ca data; the Site 999 *T. sacculifer* Mg/Ca data of Groeneveld (2005) used here to calculate $\delta^{18}O_{sw}$ were replicated at lower resolution by O'Brien et al. (2014). However, as discussed by O'Brien et al. (2014), there are notable intra- and inter-site disagreements between paleotemperature proxies in the Caribbean Sea. As one example, Groeneveld et al. (2008) found much higher (up to 7 mmol mol^{-1}) early Pliocene Mg/Ca in *T. sacculifer* at Site 1000, ~250 nautical miles to the north of Site 999; these high Mg/Ca values do not appear to result from diagenesis (Groeneveld et al., 2008). Broadly, the relative uncertainty regarding the paleotemperature history of the Caribbean Sea lends to uncertainty in its $\delta^{18}O_{sw}$ history.

Given these uncertainties, we employ a multiproxy approach to infer the early Pliocene shoaling of the Central American Seaway by identifying coeval changes in mixed layer ($\delta^{18}O_{sw}$) and thermocline (FB-δ^{15}N) proxies that are directionally consistent with predicted transport changes due to CAS shoaling, as discussed next.

4.2. Integrating Proxy Data With Modeling

To investigate how $\delta^{18}O_{sw}$ and FB-δ^{15}N would have been affected by CAS shoaling, we calculate cross-CAS volume transport in different idealized bathymetric configurations of GFDL-ESM2G (Figure 6). In *Wide*, a net eastward (Pacific to Atlantic) mass transport of 24.4 Sv is simulated across the CAS, with 8.1 Sv transported between 0 and 200 m depth and net eastward mass transport occurring at all depths down to ~1,500 m (black line in Figure 6a). In *WideShallow*, a net eastward transport of 14.7 Sv is simulated between 0 and 200 m depth (red line in Figure 6a). Thus, in GFDL-ESM2G, shoaling of the CAS from 2,000 m (*Wide*) to 200 m depth (*WideShallow*) reduces the total Pacific to Atlantic mass transport by 40% (−9.7 Sv), but it intensifies mass transport in the upper 200 m by 81% (+6.6 Sv). The intensification of Pacific-to-Atlantic flow across the CAS in response to its shoaling is directionally similar to that observed in a prior study (Sepulchre et al., 2014).

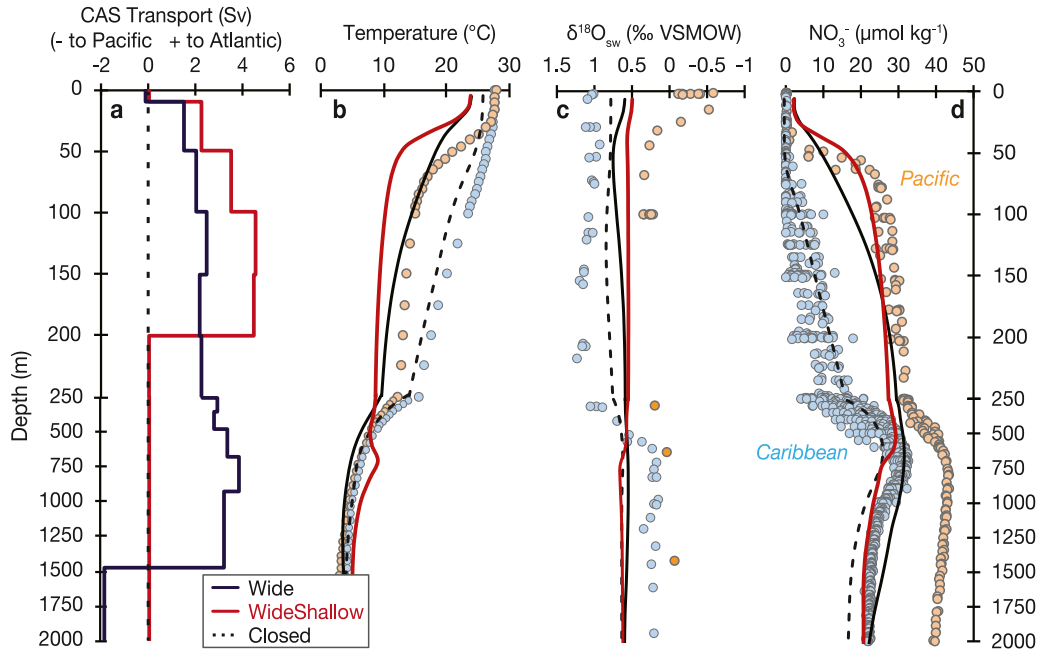

Figure 6. Interpretation of Central American Seaway history from Caribbean-Pacific oxygen and nitrogen isotope gradients. (a) Volume transport across the CAS in GFDL-ESM2G with a 2,000 m deep seaway (*Wide*, black), 200 m deep seaway (*WideShallow*, red), and closed seaway (black dashed; transports updated from Sentman et al., 2018), (b)–(d) Profiles of modern-day temperature (b, Locarnini et al., 2018) $\delta\ ^{18}O_{sw}$, (c) LeGrande & Schmidt, 2006 and nitrate concentration, and (d) Garcia et al., 2019 in the Caribbean Sea proximal to Site 999 (blue) and in the ETNP proximal to Site 1241 (orange). Lines denote temperature, nitrate concentration profiles and $\delta\ ^{18}O_{sw}$ derived from salinity (Section 2.2) at Caribbean Sea Site 999 in GFDL-ESM2G in the preindustrial control experiment (*Closed*, dashed black line), *Wide* (black line), and *WideShallow* (red line).

We illustrate how the transport change during CAS shoaling would alter the Caribbean hydrographic profiles of $\delta^{18}O_{sw}$ calculated from ESM2G output salinity (LeGrande & Schmidt, 2006) and nitrate concentration in Figures 6b and 6c, respectively. Today, the $\delta^{18}O_{sw}$ within the mixed layer (~0–60 m) at Site 999 is ~1–1.5‰ higher than within the mixed layer (~0–30 m) at Site 1241, corresponding to the higher salinity in the Caribbean Sea relative to the ETNP (LeGrande & Schmidt, 2006). Net eastward transport of surface waters with both a 2,000 and 200 m deep CAS would work to weaken this modern $\delta^{18}O_{sw}$ gradient. Notably, while Caribbean $\delta^{18}O_{sw}$ is reduced in both *Wide* and *WideShallow* compared to the *Closed* simulation, the weakest $\delta^{18}O_{sw}$ gradient between the ETNP and Caribbean is actually observed with a shoaled (200 m deep) CAS (*WideShallow*, red line in Figure 3b), and not the relatively deeper (2,000 m) CAS (*Wide*, black line in Figure 6b). This arises due to the stronger Pacific-to-Atlantic upper water column transport in the shoaled, *WideShallow* configuration (Figure 6a).

Regarding nitrate, an open CAS would have allowed the transport of high nitrate concentrations with elevated $\delta^{15}N$ from the ETNP (Figure 1) into the Caribbean, but only at depths below the ETNP mixed layer where nitrate concentrations are elevated (Figure 6c). This is observed in GFDL-ESM2G, with low nitrate concentrations in the Caribbean surface mixed layer in all scenarios but increasingly elevated subsurface Caribbean nitrate concentrations under open CAS scenarios. Specifically, the Caribbean nitrate concentration in *Wide* (black line, Figure 6c) is increased at all depths below the mixed layer and is similar to modern ETNP nitrate concentrations below 150 m depth. In *WideShallow* (red line, Figure 6c), where eastward transport is intensified in the upper 200 m (Figure 6a), Caribbean nitrate concentrations are higher still and effectively approach those observed in the modern ETNP, purportedly due to stronger thermocline inflow from the ETNP into the Caribbean (Figure 6c).

4.3. Phases of Early Pliocene CAS Shoaling

To clarify the history of mixed layer and thermocline separation between the ETNP and Caribbean Sea, we calculated gradients between the 100 kyr lowpass-filtered $\delta^{18}O_{sw}$ and FB-$\delta^{15}N$ data at Site 999 and Site 1241

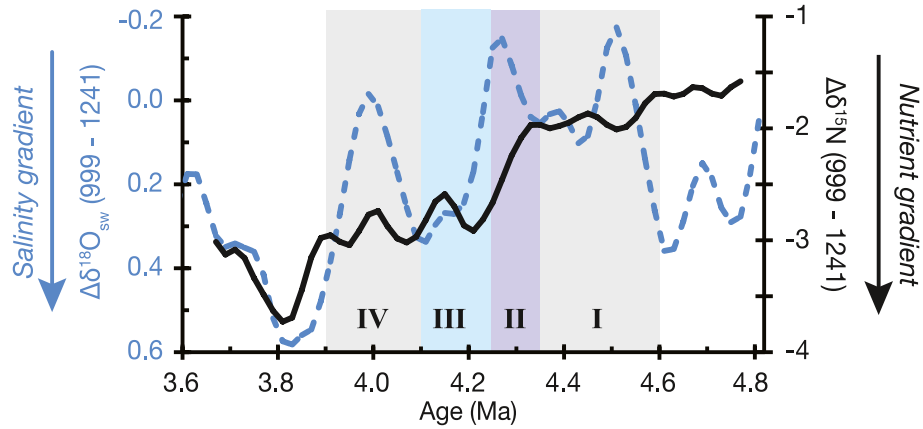

Figure 7. Isotope gradients between Sites 999 and 1241 from 4.8 to 3.6 Ma and phases of Central American Seaway shoaling. Blue dashed line is 100 kyr lowpass filtered $\delta^{18}O_{sw}$ (left axis); black solid line is FB-$\delta^{15}N$ gradient. Note that stronger gradients are plotted downward. Shaded intervals (I–IV) denote four phases of CAS shoaling described in Section 4.3.

(Figure 7). In combination, these gradients, expressed as $\Delta\delta^{18}O_{sw} = \delta^{18}O_{sw\_999}–\delta^{18}O_{sw\_1241}$ and $\Delta\delta^{15}N = \delta^{15}N_{999}–\delta^{15}N_{1241}$, respectively, delineate four phases of CAS shoaling between 4.8 and 3.9 Ma.

4.3.1. Phase 1: Initial Thermocline Nutrient Constriction (4.6–4.35 Ma)

The start of Phase 1 is denoted by the interval between 4.6 and 4.5 Ma, when the FB-$\delta^{15}N$ gradient strengthened by ~0.4‰ (with $\Delta\delta^{15}N$ declining to more negative values; Figure 7) due to a decrease in FB-$\delta^{15}N$ at Site 999 alongside little FB-$\delta^{15}N$ change at Site 1241 (Figure 4e). We interpret this to indicate a reduction in the transport of high-$\delta^{15}N$ ETNP nitrate due to initial shoaling of the CAS into thermocline depths (approaching ~50 m, Section 2.4). In the surface mixed layer, $\Delta\delta^{18}O_{sw}$ was reduced at the same time as $\Delta\delta^{15}N$ became more negative, suggesting that this initial subsurface nutrient restriction corresponded with strengthened mixed layer exchange. This observation may be explained by the tendency for shallow eastward transport across the CAS to increase as the CAS is shoaled, as occurs in GFDL-ESM2G (Figure 6a; Sentman et al., 2018) and in IPSLCM4 (Sepulchre et al., 2014). However, the small magnitude of the FB-$\delta^{15}N$ gradient (<2‰) over this time suggests that relatively vigorous subsurface nutrient transport persisted between the ETNP and Caribbean Sea.

4.3.2. Phase 2: Nutrient Isolation of the ETNP and Caribbean Sea (4.35–4.25 Ma)

Phase 2 shows a sharp and permanent (to 3.6 Ma) ~1‰ increase in the FB-$\delta^{15}N$ gradient toward $\Delta\delta^{15}N$ values of ~−3‰ (Figure 7). We interpret this to indicate the isolation of the Caribbean thermocline nitrate pool from the ETNP thermocline nitrate pool. This would require that the CAS was sufficiently shoaled (to ≤50 m depth, Section 2.4) to effectively cease large-scale thermocline exchange by 4.25 Ma. In the surface mixed layer, lower $\Delta\delta^{18}O_{sw}$ again corresponded with more negative $\Delta\delta^{15}N$, as was observed in Phase 1. Thus, we infer that shoaling of the CAS to ~50 m depth between 4.35 and 4.25 Ma shut off subsurface nutrient transport but correspondingly intensified the transport of surface mixed layer waters from the ETNP to the Caribbean.

4.3.3. Phase 3: Reduced Surface Mixed Layer Transport (4.25–4.1 Ma)

Following the establishment of a ~3‰ FB-$\delta^{15}N$ gradient starting at 4.25 Ma, $\Delta\delta^{18}O_{sw}$ rapidly increased by ~0.4‰. The end of Phase 3 by 4.1 Ma marked the first cooccurrence of large positive $\Delta\delta^{18}O_{sw}$ with large negative $\Delta\delta^{15}N$ (Figure 7). These coeval clues for higher salinity within, and an absence of ETNP nutrients below, the Caribbean Sea mixed layer suggests that both thermocline and mixed-layer waters in the ETNP and Caribbean became effectively isolated by 4.1 Ma.

4.3.4. Phase 4: Reduction of the $\delta^{18}O_{sw}$ Gradient (4.1–3.9 Ma)

Between 4.1 and 4.0 Ma, $\Delta\delta^{18}O_{sw}$ declined while $\Delta\delta^{15}N$ remained constant. This fourth phase could either be interpreted as a deepening of the CAS only to mixed-layer depths, such that fresher ETNP mixed layer waters

once again flowed into the Caribbean Sea but high-$\delta^{15}N$ ETNP thermocline nitrate did not. Alternatively, the $\Delta\delta^{18}O_{sw}$ decline could reflect local hydrographic effects unrelated to CAS transport that lowered mixed layer salinity in the Caribbean Sea, such as presumably occurred earlier between 4.6 and 4.8 Ma when $\Delta\delta^{18}O_{sw}$ varied while $\Delta\delta^{15}N$ was unchanged (Figure 7; Steph, Tiedemann, Prange, et al., 2006).

We note that a subsequent transient strengthening of the $\delta^{18}O_{sw}$ and FB-$\delta^{15}N$ gradients occurred around 3.8 Ma. This $\Delta\delta^{18}O_{sw}$ increase was driven by a further increase in Caribbean Sea $\delta^{18}O_{sw}$ with near-constant ETNP $\delta^{18}O_{sw}$ (Figure 4d), which could be explained as a salinity increase in the Caribbean Sea unrelated to CAS history. However, the stronger FB-$\delta^{15}N$ gradient appears to result from a single elevated FB-$\delta^{15}N$ value at Site 1241 (8.9‰ at 3.81 Ma) and limited sample availability over this interval, with only two Site 1241 FB-$\delta^{15}N$ data between 3.76 and 3.86 Ma (Figure 4e). Further, Site 999 shows no significant change in FB-$\delta^{15}N$ around this interval relative to measurement precision (Figure 4e). Accordingly, we suggest that the expanded FB-$\delta^{15}N$ gradient at 3.8 Ma was driven by an increase of the $\delta^{15}N$ of ETNP nitrate independent of the CAS, and/or was an artifact of aliasing across low resolution sampling. Thus, we do not interpret the expanded FB-$\delta^{15}N$ gradient at 3.8 Ma as reflecting further CAS shoaling. This is additionally supported by the return to a ~3‰ FB-$\delta^{15}N$ gradient after 3.75 Ma when the sampling resolution of Site 1241 increases (Figures 4e and 7). This feature can be further investigated with higher-resolution FB-$\delta^{15}N$ sampling of Site 1241.

In summary, the FB-$\delta^{15}N$ data show that the large-scale eastward subsurface nutrient transport across the CAS was progressively constricted after 4.8 Ma and largely ceased by 4.25 Ma. This indicates that, from the perspective of Site 999 in the Caribbean Sea, the CAS had shoaled to only allow for the transport of nutrient-poor mixed layer waters by 4.25 Ma. In contrast, the mixed layer $\delta^{18}O_{sw}$ gradient between Sites 999 and 1241 is more dynamic throughout the Early Pliocene, with high amplitude $\Delta\delta^{18}O_{sw}$ variations occurring before 4.6 Ma. Thus, it appears that local hydrological changes within the Caribbean Sea and ETNP may have a substantial impact on $\delta^{18}O_{sw}$, comparable to or exceeding the impact of CAS shoaling on $\delta^{18}O_{sw}$ (e.g., Steph, Tiedemann, Prange, et al., 2006).

4.4. Implications for Central American Seaway History

The FB-$\delta^{15}N$ and $\delta^{18}O_{sw}$ gradients help contextualize existing proxies that have been interpreted to reflect CAS shoaling throughout the water column (Figure 8). Starting from the deep ocean, neodymium (Nd) isotopes in fish teeth and bulk sediment leachates show that the deep waters in the Caribbean and ETNP became isotopically distinct around 10 Ma and maintained a large Nd isotope separation over the early Pliocene (Newkirk & Martin, 2009; Osborne et al., 2014). On the basis of lower-resolution modeling with IPSLCM4 (1°–2° grid vs. 0.33°–1° grid in ESM2G), Sepulchre et al. (2014) concluded that the Pacific-Caribbean Nd isotope separation required a shoaling of the CAS to ~50–200 m depth around 10 Ma. Although we lack data prior to 5.3 Ma, elevated FB-$\delta^{15}N$ in the Caribbean Sea and its small difference relative to the ETNP from 5.3 to 4.35 Ma indicate that the CAS was not yet sufficiently shoaled to restrict thermocline nutrient exchange in the earliest Pliocene. Together, the Nd and N isotopes suggest that the CAS was relatively shallow (between ~50 and 200 m) for a ~6 million period between the late Miocene and early Pliocene. The extent to which the CAS shoaled to thermocline depths during this interval could be further tested with late Miocene FB-$\delta^{15}N$ records from the ETNP and Caribbean Sea.

After 4.6 Ma, the established Pacific-Caribbean Nd isotope gradient was joined by an emergent FB-$\delta^{15}N$ gradient, indicating that additional CAS shoaling restricted thermocline water exchange between the Pacific and Caribbean. Regarding the surface mixed layer, although the $\delta^{18}O_{sw}$ gradient is likely influenced by local hydrographic changes (Steph, Tiedemann, Prange, et al., 2006, and this study), its use as a proxy for CAS mixed layer exchange is supported by the inferences on thermocline nutrient exchange from the FB-$\delta^{15}N$ gradient. In particular, the coeval strengthening of the FB-$\delta^{15}N$ gradient and reduction of the $\delta^{18}O_{sw}$ gradient from 4.6 to 4.5 Ma and 4.35 to 4.25 Ma aligns with model expectations for stronger upper ocean transport across the CAS, and thus a reduced $\delta^{18}O_{sw}$ gradient, with CAS shoaling (Figure 5 and Sepulchre et al., 2014). More broadly, the co-occurring enhancement of FB-$\delta^{15}N$ and $\delta^{18}O_{sw}$ gradients between the Caribbean and ETNP between 4.35 and 4.1 Ma denote this time as an interval of pronounced CAS shoaling and restricted exchange at both thermocline and mixed layer depths.

The final closure of the remaining surface water connections across the Panama Arc, and thus the CAS sensu stricto, remains notoriously challenging to date. For instance, complete closure of the CAS has been assigned to ~3.3 Ma (Marine Isotope Stage [MIS] M2) from $\delta^{18}O_{sw}$ and dinoflagellate cyst productivity reconstructions in

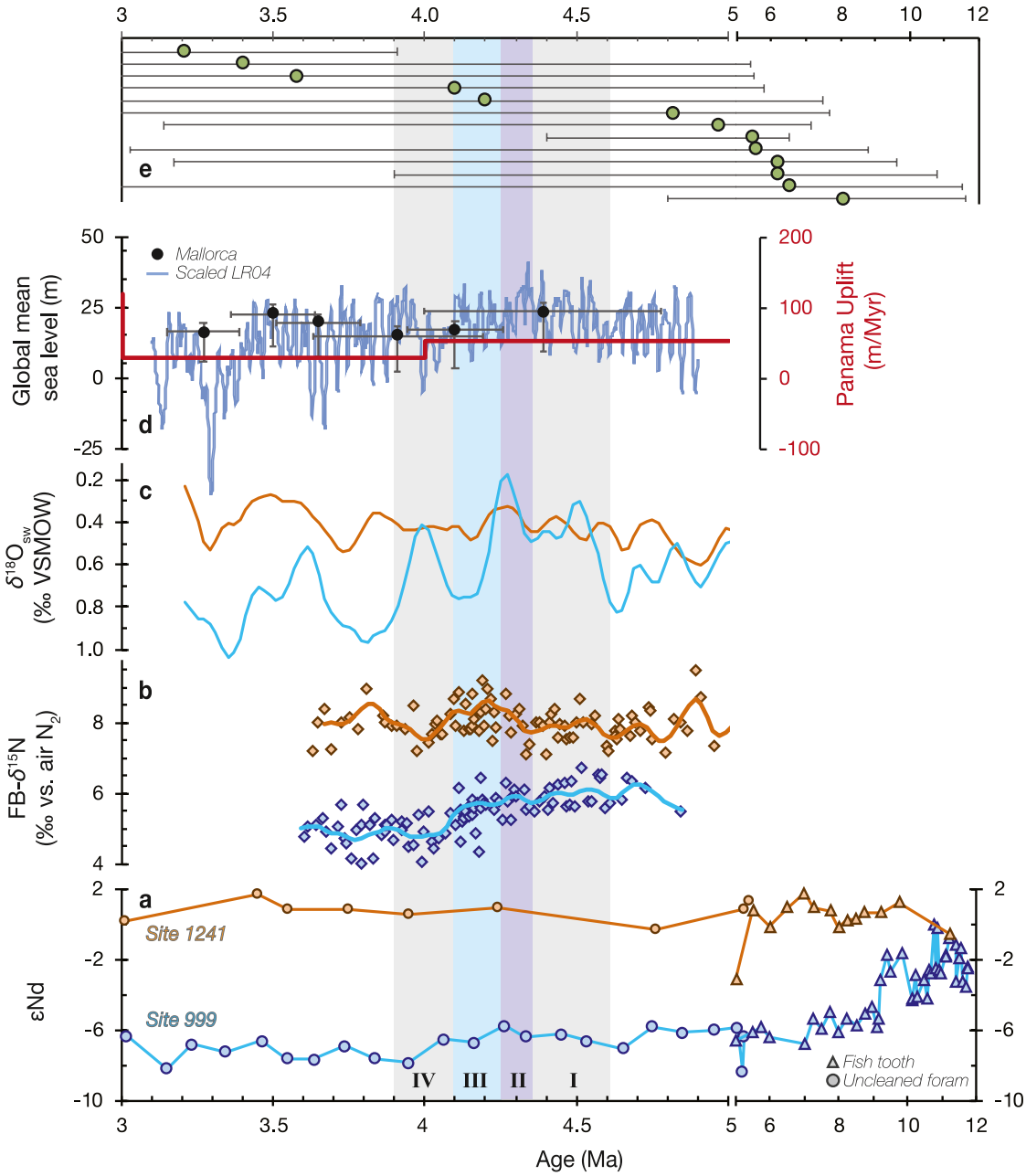

Figure 8. A deep-to-surface view of Central American Seaway shoaling. (a) At bottom, Nd isotopic composition (in epsilon units) of fossil fish teeth (triangles, Newkirk & Martin, 2009) and uncleaned foraminifera (circles, Osborne et al., 2014), (b) FB-δ^{15}N (diamonds) from Site 1241 and Site 999 and 100 kyr lowpass filters, (c) 100 kyr lowpass filters of $\delta^{18}O_{sw}$. Orange/blue lines and symbols in (a)–(c) denote Site 1241/999 data, respectively, (d) Global mean sea level from U-Pb dated phreatic overgrowths on Mallorcan speleothems (black circles) and based on ice volume changes calculated from the LR04 δ^{18}O stack (blue curve) (Dumitru et al., 2019), and (e) Median molecular divergence ages (green circles) for taxa calculated by O'Dea et al. (2016). Error bars indicate 95% highest posterior density (HPD) age ranges; uncapped error bars at left extend after 3.0 Ma. Only divergences where the 97.5% highest posterior density (HPD) age falls within the last 12 Myr are shown. Shaded intervals (I–IV) denote four phases of CAS shoaling described in Section 4.2 and shown on Figure 7.

the Caribbean Sea (De Schepper et al., 2013), approximately 3.2 Ma from molecular records of marine taxa divergence between the Pacific and Caribbean (Figure 8e; O'Dea et al., 2016), and ~2.5 Ma (MIS 100 and 98) on the basis of Caribbean SST warming and thermocline deepening (Groeneveld et al., 2014). Regarding the molecular records, dating species divergences based on molecular clock approaches is subject to large age uncertainties in comparison to marine sediment reconstructions. For instance, of the 38 sister taxa whose molecular divergence was dated and compiled by O'Dea et al. (2016), the median divergence age of only four taxa fall

within the early Pliocene interval of our study (5.3–3.6 Ma), and with divergence age uncertainty averaging ±1.1 Ma (Figure 8e). Thus, a confident alignment of marine species divergence with the sequence of shoaling events indicated by the FB-$\delta^{15}N$ and $\delta^{18}O_{sw}$ gradients requires order-of-magnitude improvements in the precision of molecular divergence age estimates.

Our records indicate that the ETNP and Caribbean surface mixed layer and thermocline properties were separated by 4.1 Ma, and maintained separation through 3.6 Ma. Although our paired FB-$\delta^{15}N$ records do not yet extend after 3.6 Ma, it is noteworthy that a large $\delta^{18}O_{sw}$ gradient was maintained through 3.2 Ma (Figure 8c). These data are difficult to reconcile with estimates of a later final CAS closure at ∼3.3 Ma (De Schepper et al., 2013) or ∼2.5 Ma (Groeneveld et al., 2014). Moreover, these younger CAS closure dates are also inconsistent with the broader geologic drivers of sea level fall across the Central American Seaway during the early Pliocene. Sedimentary units from the Panama Arc indicate continual uplift (on order of ∼100 m/Myr) after 6 Ma (Figure 8d; O'Dea et al., 2016), possibly a consequence of slab window formation beneath the Panama Isthmus after 8 Ma (McGirr et al., 2021). Additionally, although Pliocene sea level remains subject to uncertainty (Raymo et al., 2018), sea-level datums and benthic $\delta^{18}O$-based sea-level estimates consistent with these datums (Dumitru et al., 2019) indicate a small, gradual decline in sea-level highstands over the late Pliocene (Figure 8d). Thus, in the context of our proxy records indicating a Pacific-Caribbean separation of thermocline and surface mixed layer waters by 4.1 Ma, ongoing uplift of the Panama Arc, and steady or declining global mean sea level, it is difficult to envisage how the CAS could have allowed for significant Pacific inflows to the Caribbean after 4.1 Ma.

5. Conclusions

We reconstructed the exchange of subsurface nutrients and surface waters between the Caribbean Sea and the eastern tropical North Pacific Ocean (ETNP) using planktonic foraminifera-bound nitrogen isotopes and the oxygen isotopic composition of seawater derived from paired $\delta^{18}O$ and Mg/Ca of planktonic foraminifera. Our results indicate that subsurface nutrient transport across the CAS was restricted by 4.25 Ma, suggesting that the CAS shoaled to an estimated depth of 50 m at this time. This subsurface nutrient constriction was followed by an increase in the $\delta^{18}O_{sw}$ difference between the Caribbean and ETNP by 4.1 Ma.

Two caveats of our approach should be mentioned as motivation for future work. First, the $\delta^{18}O_{sw}$ gradient is small and dynamic across our study interval. This makes it difficult to ascertain the extent to which local hydrology modified the $\delta^{18}O_{sw}$ of Caribbean and/or ETNP mixed layer waters independent of their exchange across the CAS, and also underscores the importance of precise paleotemperature estimates to deconvolve $\delta^{18}O_{pf}$ into $\delta^{18}O_{sw}$. Second, although we interpret the FB-$\delta^{15}N$ changes at Site 999 as representative of direct nutrient transport from the ETNP to the Caribbean, FB-$\delta^{15}N$ variations at Site 999 could also be generated indirectly if CAS shoaling impacted the rate of nitrogen fixation in the tropical Atlantic Ocean. Additional studies of early Pliocene FB-$\delta^{15}N$ from locations not directly impacted by CAS transport would help illuminate this possibility. Nonetheless, the most parsimonious explanation for the strong gradients that emerged between the ETNP and the Caribbean in both thermocline and surface water proxies by 4.1 Ma is that the CAS had sufficiently shoaled to restrict large-scale oceanographic flows at this time.

Our interpretation of significant shoaling of the CAS at 4.1 Ma predates the interpreted closure of the CAS at 3.2 Ma based on revised analyses of molecular divergence between sister taxa of shallow-water marine organisms (O'Dea et al., 2016). However, in addition to allowing for the large dating uncertainty on molecular divergence estimates, we stress that these two data sources provide information on different aspects of CAS history. The FB-$\delta^{15}N$ and $\delta^{18}O_{sw}$ reconstructions from open ocean Sites 999 and 1241 track the large-scale, climatically relevant movement of seawater and dissolved nutrients between the Pacific and Atlantic basins. These deep-sea sediment records, distal from coastal areas in the Panama Arc, would likely be insensitive to the last vestiges of Pacific-to-Atlantic exchange. While small passageways through the Panama Arc could have facilitated the exchange of shallow-water marine populations between the ETNP and Caribbean, they would not have transported sufficient quantities of low-salinity seawater or nutrients to be detectable at Site 999. In summary, while the Isthmus of Panama may not have fully formed until 3.2 Ma or later, our records denote 4.1 Ma as the end of climatically significant oceanographic transport across the Central American Seaway.

Data Availability Statement

New foraminifera-bound nitrogen isotope data and oxygen isotopic composition of seawater reconstructions generated in this study are published at PANGAEA (Farmer, Martínez-García, et al., 2025).

Acknowledgments
We thank Florian Rubach, Barbara Hinnenberg, and Nicolas Duprey for laboratory assistance at MPIC, and Yeongjun Ryu for providing additional North Atlantic nitrate isotope data shown in Figure 1. JRF, AMG, RS, AA, MY, and GHH were funded by the Max Planck Society. JRF and DMS also acknowledge support from NSF OCE-2303549 and 2303548, respectively, and the Tuttle Fund of the Department of Geosciences at Princeton University.

References

Antonov, J. I., Locarnini, R. A., Boyer, T. P., Mishonov, A. V., & Garcia, H. E. (2006). World Ocean Atlas 2005, volume 2: Salinity. In S. Levitus (Ed.), *NOAA Atlas NESDIS 62* (p. 182). U.S. Government Printing Office.

Auderset, A., Fripiat, F., Creel, R. C., Oesch, L., Studer, A. S., Repschläger, J., et al. (2024). Sea level modulation of Atlantic nitrogen fixation over glacial cycles. *Paleoceanography and Paleoclimatology*, *39*(8), e2024PA004878. https://doi.org/10.1029/2024pa004878

Bacon, C. D., Silvestro, D., Jaramillo, C., Smith, B. T., Chakrabarty, P., & Antonelli, A. (2015). Biological evidence supports an early and complex emergence of the Isthmus of Panama. *Proceedings of the National Academy of Sciences*, *112*(19), 6110–6115. https://doi.org/10.1073/pnas.1423853112

Casciotti, K. L. (2016). Nitrogen and oxygen isotopic studies of the marine nitrogen cycle. *Annual Review of Marine Science*, *8*(1), 379–407. https://doi.org/10.1146/annurev-marine-010213-135052

Cline, J. D., & Kaplan, I. R. (1975). Isotopic fractionation of dissolved nitrate during denitrification in the eastern tropical North Pacific Ocean. *Marine Chemistry*, *3*(4), 271–299. https://doi.org/10.1016/0304-4203(75)90009-2

Coates, A. G., Collins, L. S., Aubry, M. P., & Berggren, W. A. (2004). The geology of the Darien, Panama, and the late Miocene-Pliocene collision of the Panama arc with northwestern South America. *Geological Society of America Bulletin*, *116*(11–12), 1327–1344. https://doi.org/10.1130/b25275.1

Dekens, P. S., Lea, D. W., Pak, D. K., & Spero, H. J. (2002). Core top calibration of Mg/Ca in tropical foraminifera: Refining paleotemperature estimation. *Geochemistry, Geophysics, Geosystems*, *3*(4), 1–29. https://doi.org/10.1029/2001gc000200

Dekens, P. S., Ravelo, A. C., & McCarthy, M. D. (2007). Warm upwelling regions in the Pliocene warm period. *Paleoceanography*, *22*(3). https://doi.org/10.1029/2006PA001394

De Schepper, S., Groeneveld, J., Naafs, B. D. A., Van Renterghem, C., Hennissen, J., Head, M. J., et al. (2013). Northern hemisphere glaciation during the globally warm early late Pliocene. *PLoS One*, *8*(12), e81508. https://doi.org/10.1371/journal.pone.0081508

Dumitru, O. A., Austermann, J., Polyak, V. J., Fornós, J. J., Asmerom, Y., Ginés, J., et al. (2019). Constraints on global mean sea level during Pliocene warmth. *Nature*, *574*(7777), 233–236. https://doi.org/10.1038/s41586-019-1543-2

Dunne, J. P., John, J. G., Adcroft, A. J., Griffies, S. M., Hallberg, R. W., Shevliakova, E., et al. (2012). GFDL's ESM2 global coupled climate–carbon earth system models. Part I: Physical formulation and baseline simulation characteristics. *Journal of Climate*, *25*(19), 6646–6665. https://doi.org/10.1175/jcli-d-11-00560.1

Dunne, J. P., John, J. G., Shevliakova, E., Stouffer, R. J., Krasting, J. P., Malyshev, S. L., et al. (2013). GFDL's ESM2 global coupled climate–carbon earth system models. Part II: Carbon system formulation and baseline simulation characteristics. *Journal of Climate*, *26*(7), 2247–2267. https://doi.org/10.1175/jcli-d-12-00150.1

Emile-Geay, J. (2015). Common-climate: Preliminary release (v0.1). *Zenodo*. https://doi.org/10.5281/zenodo.32474

Eppley, R. W., & Peterson, B. J. (1979). Particulate organic matter flux and planktonic new production in the deep ocean. *Nature*, *282*(5740), 677–680. https://doi.org/10.1038/282677a0

Farmer, J. R., Fehrenbacher, J. S., Horner, T. J., & Kast, E. R. (2025). Tools to trace past productivity and ocean nutrients. 3rd Edition. *Treatise of Geochemistry*, 41–151. https://doi.org/10.1016/B978-0-323-99762-1.00039-5

Farmer, J. R., Martínez-García, A., Sentman, L., Schiebel, R., Arns, A., Yehudai, M., et al. (2025). Early Pliocene foraminifera-bound nitrogen isotopes and oxygen isotopic composition of seawater from ODP Sites 999 and 1241 [Dataset bundled publication]. *PANGAEA*. https://doi.org/10.1594/PANGAEA.974971

Farmer, J. R., Pico, T., Underwood, O. M., Cleveland Stout, R., Granger, J., Cronin, T. M., et al. (2023). The Bering Strait was flooded 10,000 years before the last glacial maximum. *Proceedings of the National Academy of Sciences*, *120*(1), e2206742119. https://doi.org/10.1073/pnas.2206742119

Farmer, J. R., Sigman, D. M., Granger, J., Underwood, O. M., Fripiat, F., Cronin, T. M., et al. (2021). Arctic Ocean stratification set by sea level and freshwater inputs since the last ice age. *Nature Geoscience*, *14*(9), 684–689. https://doi.org/10.1038/s41561-021-00789-y

Ford, H. L., Ravelo, A. C., & Hovan, S. (2012). A deep Eastern Equatorial Pacific thermocline during the early Pliocene warm period. *Earth and Planetary Science Letters*, *355*, 152–161. https://doi.org/10.1016/j.epsl.2012.08.027

Fripiat, F., Marconi, D., Rafter, P., Sigman, D. M., Altabet, M. A., Bourbonnais, A., et al. (2021). Compilation of nitrate $\delta^{15}N$ in the ocean [Dataset]. *PANGAEA*. https://doi.org/10.1594/PANGAEA.936484

Garcia, H. E., Locarnini, R. A., Boyer, T. P., & Antonov, J. I. (2006a). World Ocean Atlas 2005, volume 3: Dissolved Oxygen, apparent Oxygen utilization, and Oxygen saturation. In S. Levitus (Ed.), *NOAA Atlas NESDIS 63* (p. 342). U.S. Government Printing Office.

Garcia, H. E., Locarnini, R. A., Boyer, T. P., & Antonov, J. I. (2006b). World Ocean Atlas 2005, volume 4: Nutrients (phosphate, nitrate, silicate). In S. Levitus (Ed.), *NOAA Atlas NESDIS 64* (p. 396). U.S. Government Printing Office.

Garcia, H. E., Weathers, K. W., Paver, C. R., Smolyar, I., Boyer, T. P., Locarnini, M. M., & Seidov, D. (2019). In A. Mishonov Technical (Ed.), *World Ocean Atlas 2018. Vol. 4: Dissolved inorganic nutrients (phosphate, nitrate and nitrate+ nitrite, silicate)* (p. 35). NOAA Atlas NESDIS 84.

Gray, W. R., & Evans, D. (2019). Nonthermal influences on Mg/Ca in planktonic foraminifera: A review of culture studies and application to the last glacial maximum. *Paleoceanography and Paleoclimatology*, *34*(3), 306–315. https://doi.org/10.1029/2018pa003517

Groeneveld, J. (2005). *Effect of the Pliocene closure of the Panamanian Gateway on Caribbean and east Pacific sea surface temperatures and salinities by applying combined Mg/Ca and $\delta^{18}O$ measurements (5.6-2.2 Ma)* (Doctoral dissertation). Christian-Albrechts-Universität Kiel.

Groeneveld, J., Hathorne, E. C., Steinke, S., DeBey, H., Mackensen, A., & Tiedemann, R. (2014). Glacial induced closure of the Panamanian gateway during Marine Isotope Stages (MIS) 95–100 (~ 2.5 Ma). *Earth and Planetary Science Letters*, *404*, 296–306. https://doi.org/10.1016/j.epsl.2014.08.007

Groeneveld, J., Nürnberg, D., Tiedemann, R., Reichart, G.-J., Steph, S., Reuning, L., et al. (2008). Foraminiferal Mg/Ca increase in the Caribbean during the Pliocene: Western Atlantic warm pool formation, salinity influence, or diagenetic overprint? *Geochemistry, Geophysics, Geosystems*, *9*(1), Q01P23. https://doi.org/10.1029/2006GC001564

Groeneveld, J., Steph, S., Tiedemann, R., Garbe-Schönberg, C., Nürnberg, D., & Sturm, A. (2006). Pliocene mixed-layer oceanography for Site 1241, using combined Mg/Ca and $\delta^{18}O$ analyses of Globigerinoides sacculifer. In *In proceedings of the Ocean Drilling Program: Scientific results* (Vol. 202, pp. 1–27). Texas A&M University.

Haug, G. H., & Tiedemann, R. (1998). Effect of the formation of the isthmus of Panama on Atlantic Ocean thermohaline circulation. *Nature*, *393*(6686), 673–676. https://doi.org/10.1038/31447

Haug, G. H., Tiedemann, R., Zahn, R., & Ravelo, A. C. (2001). Role of Panama uplift on oceanic freshwater balance. *Geology*, *29*(3), 207–210. https://doi.org/10.1130/0091-7613(2001)029<0207:ropuoo>2.0.co;2

Holte, J., Talley, L. D., Gilson, J., & Roemmich, D. (2017). An Argo mixed layer climatology and database. *Geophysical Research Letters*, *44*(11), 5618–5626. https://doi.org/10.1002/2017gl073426

Keigwin, L. (1982). Isotopic paleoceanography of the Caribbean and East Pacific: Role of Panama uplift in late Neogene time. *Science*, *217*(4557), 350–353. https://doi.org/10.1126/science.217.4557.350

Key, R. M., Kozyr, A., Sabine, C. L., Lee, K., Wanninkhof, R., Bullister, J. L., et al. (2004). A global ocean carbon climatology: Results from global data analysis Project (GLODAP). *Global Biogeochemical Cycles*, *18*(4), GB4031. https://doi.org/10.1029/2004GB002247

Khon, V. C., Hoogakker, B. A. A., Schneider, B., Segschneider, J., & Park, W. (2023). Effect of an open Central American Seaway on ocean circulation and the oxygen minimum zone in the tropical Pacific from model simulations. *Geophysical Research Letters*, *50*(20), e2023GL103728. https://doi.org/10.1029/2023gl103728

Knapp, A. N., Sigman, D. M., & Lipschultz, F. (2005). N isotopic composition of dissolved organic nitrogen and nitrate at the Bermuda Atlantic Time-series Study site. *Global Biogeochemical Cycles*, *19*(1). https://doi.org/10.1029/2004GB002320

Kwiecinski, J. V., & Babbin, A. R. (2021). A high-resolution Atlas of the eastern tropical pacific oxygen deficient zones. *Global Biogeochemical Cycles*, *35*(12), e2021GB007001. https://doi.org/10.1029/2021gb007001

Lear, C. H., Rosenthal, Y., & Wright, J. D. (2003). The closing of a seaway: Ocean water masses and global climate change. *Earth and Planetary Science Letters*, *210*(3–4), 425–436. https://doi.org/10.1016/s0012-821x(03)00164-x

LeGrande, A. N., & Schmidt, G. A. (2006). Global gridded data set of the oxygen isotopic composition in seawater. *Geophysical Research Letters*, *33*(12). https://doi.org/10.1029/2006GL026011

Lessios, H. A. (2008). The great American schism: Divergence of marine organisms after the rise of the central American isthmus. *Annual Review of Ecology Evolution and Systematics*, *39*(1), 63–91. https://doi.org/10.1146/annurev.ecolsys.38.091206.095815

Lisiecki, L. E., & Raymo, M. E. (2005). A Pliocene-Pleistocene stack of 57 globally distributed benthic $\delta^{18}O$ records. *Paleoceanography*, *20*(1), PA1003. https://doi.org/10.1029/2004PA001071

Liu, Z., Altabet, M. A., & Herbert, T. D. (2008). Plio-pleistocene denitrification in the eastern tropical North Pacific: Intensification at 2.1 Ma. *Geochemistry, Geophysics, Geosystems*, *9*(11). https://doi.org/10.1029/2008GC002044

Locarnini, R. A., Mishonov, A. V., Antonov, J. I., Boyer, T. P., & Garcia, H. E. (2006). World Ocean Atlas 2005, volume 1: Temperature. In S. Levitus (Ed.), *NOAA Atlas NESDIS 61* (p. 182). U.S. Government Printing Office.

Locarnini, R. A., Mishonov, A. V., Baranova, O. K., Boyer, T. P., Zweng, M. M., Garcia, H. E., et al. (2018). World Ocean Atlas 2018, volume 1: Temperature. In A. Mishonov (Ed.), *NOAA Atlas NESDIS 81* (p. 52). U.S. Government Printing Office.

Lunt, D. J., Valdes, P. J., Haywood, A., & Rutt, I. C. (2008). Closure of the Panama seaway during the Pliocene: Implications for climate and northern hemisphere glaciation. *Climate Dynamics*, *30*, 1–18. https://doi.org/10.1007/s00382-007-0265-6

Marconi, D., Sigman, D. M., Casciotti, K. L., Campbell, E. C., Weigand, M. A., Fawcett, S. E., et al. (2017). Tropical dominance of N_2 fixation in the North Atlantic Ocean. *Global Biogeochemical Cycles*, *31*(10), 1608–1623. https://doi.org/10.1002/2016gb005613

Martínez-García, A., Jung, J., Ai, X. E., Sigman, D. M., Auderset, A., Duprey, N. N., et al. (2022). Laboratory assessment of the impact of chemical oxidation, mineral dissolution, and heating on the nitrogen isotopic composition of fossil-bound organic matter. *Geochemistry, Geophysics, Geosystems*, *23*(8), e2022GC010396. https://doi.org/10.1029/2022gc010396

McGirr, R., Seton, M., & Williams, S. (2021). Kinematic and geodynamic evolution of the Isthmus of Panama region: Implications for central American seaway closure. *GSA Bulletin*, *133*(3–4), 867–884. https://doi.org/10.1130/b35595.1

Molnar, P. (2008). Closing of the central American seaway and the ice age: A critical review. *Paleoceanography*, *23*(2). https://doi.org/10.1029/2007pa001574

Montes, C., Bayona, G., Cardona, A., Buchs, D., Silva, C. A., Moron, S., et al. (2012). Arc-continent collision and orocline formation: Closing of the central American seaway. *Journal of Geophysical Research*, *117*(B4), B04105. https://doi.org/10.1029/2011JB008959

Montes, C., Cardona, A., Jaramillo, C., Pardo, A., Silva, J. C., Valencia, V., et al. (2015). Middle Miocene closure of the central American seaway. *Science*, *348*(6231), 226–229. https://doi.org/10.1126/science.aaa2815

Moretti, S., Duprey, N. N., Foreman, A. D., Arns, A., Brömme, S., Jung, J., et al. (2024). Analytical improvements and assessment of long-term performance of the oxidation–denitrifier method. *Rapid Communications in Mass Spectrometry*, *38*(1), e9650. https://doi.org/10.1002/rcm.9650

Newkirk, D. R., & Martin, E. E. (2009). Circulation through the central American seaway during the Miocene carbonate crash. *Geology*, *37*(1), 87–90. https://doi.org/10.1130/g25193a.1

O'Brien, C. L., Foster, G. L., Martínez-Botí, M. A., Abell, R., Rae, J. W., & Pancost, R. D. (2014). High sea surface temperatures in tropical warm pools during the Pliocene. *Nature Geoscience*, *7*(8), 606–611. https://doi.org/10.1038/ngeo2194

O'Dea, A., Lessios, H. A., Coates, A. G., Eytan, R. I., Restrepo-Moreno, S. A., Cione, A. L., et al. (2016). Formation of the isthmus of Panama. *Science Advances*, *2*(8), e1600883. https://doi.org/10.1126/sciadv.1600883

Öğretmen, N., Schiebel, R., Jochum, K. P., Stoll, B., Weis, U., Repschläger, J., et al. (2020). Deep thermohaline circulation across the closure of the Central American Seaway. *Paleoceanography and Paleoclimatology*, *35*(12), e2020PA004049. https://doi.org/10.1029/2020pa004049

Osborne, A. H., Newkirk, D. R., Groeneveld, J., Martin, E. E., Tiedemann, R., & Frank, M. (2014). The seawater neodymium and lead isotope record of the final stages of Central American Seaway closure. *Paleoceanography*, *29*(7), 715–729. https://doi.org/10.1002/2014pa002676

Rafter, P. A., Bagnell, A., Marconi, D., & DeVries, T. (2019). Global trends in marine nitrate N isotopes from observations and a neural network-based climatology. *Biogeosciences*, *16*(13), 2617–2633. https://doi.org/10.5194/bg-16-2617-2019

Rafter, P. A., Sigman, D. M., Charles, C. D., Kaiser, J., & Haug, G. H. (2012). Subsurface tropical Pacific nitrogen isotopic composition of nitrate: Biogeochemical signals and their transport. *Global Biogeochemical Cycles*, *26*(1), GB1003. https://doi.org/10.1029/2010gb003979

Raymo, M. E., Kozdon, R., Evans, D., Lisiecki, L., & Ford, H. L. (2018). The accuracy of mid-Pliocene $\delta^{18}O$-based ice volume and sea level reconstructions. *Earth-Science Reviews*, *177*, 291–302. https://doi.org/10.1016/j.earscirev.2017.11.022

Ren, H., Sigman, D. M., Thunell, R. C., & Prokopenko, M. G. (2012). Nitrogen isotopic composition of planktonic foraminifera from the modern ocean and recent sediments. *Limnology & Oceanography*, *57*(4), 1011–1024. https://doi.org/10.4319/lo.2012.57.4.1011

Saito, T. (1976). Geologic significance of coiling direction in the planktonic foraminifera Pulleniatina. *Geology*, *4*(5), 305–309. https://doi.org/10.1130/0091-7613(1976)4<305:gsocdi>2.0.co;2

Schiebel, R., Smart, S. M., Jentzen, A., Jonkers, L., Morard, R., Meilland, J., et al. (2018). Advances in planktonic foraminifer research: New perspectives for paleoceanography. *Revue de Micropaleontologie*, *61*(3–4), 113–138. https://doi.org/10.1016/j.revmic.2018.10.001

Sentman, L. T., Dunne, J. P., Stouffer, R. J., Krasting, J. P., Toggweiler, J. R., & Broccoli, A. J. (2018). The mechanistic role of the Central American seaway in a GFDL Earth System model. Part 1: Impacts on global ocean mean state and circulation. *Paleoceanography and Paleoclimatology*, *33*(7), 840–859. https://doi.org/10.1029/2018pa003364

Sepulchre, P., Arsouze, T., Donnadieu, Y., Dutay, J. C., Jaramillo, C., Le Bras, J., et al. (2014). Consequences of shoaling of the Central American Seaway determined from modeling Nd isotopes. *Paleoceanography*, *29*(3), 176–189. https://doi.org/10.1002/2013pa002501

Sigman, D. M., Casciotti, K. L., Andreani, M., Barford, C., Galanter, M. B. J. K., & Böhlke, J. K. (2001). A bacterial method for the nitrogen isotopic analysis of nitrate in seawater and freshwater. *Analytical Chemistry*, *73*(17), 4145–4153. https://doi.org/10.1021/ac010088e

Sigman, D. M., Granger, J., DiFiore, P. J., Lehmann, M. M., Ho, R., Cane, G., & Van Geen, A. (2005). Coupled nitrogen and oxygen isotope measurements of nitrate along the eastern North Pacific margin. *Global Biogeochemical Cycles*, *19*(4). https://doi.org/10.1029/2005gb002458

Smart, S. M., Ren, H., Fawcett, S. E., Schiebel, R., Conte, M., Rafter, P. A., et al. (2018). Ground-truthing the planktic foraminifer-bound nitrogen isotope paleo-proxy in the Sargasso Sea. *Geochimica et Cosmochimica Acta*, *235*, 463–482. https://doi.org/10.1016/j.gca.2018.05.023

Spezzaferri, S., Kucera, M., Pearson, P. N., Wade, B. S., Rappo, S., Poole, C. R., et al. (2015). Fossil and genetic evidence for the polyphyletic nature of the planktonic foraminifera "*Globigerinoides*", and description of the new genus *Trilobatus*. *PLoS One*, *10*(5), e0128108. https://doi.org/10.1371/journal.pone.0128108

Steph, S., Tiedemann, R., Groeneveld, J., Sturm, A., & Nürnberg, D. (2006). Pliocene changes in tropical east Pacific upper ocean stratification: Response to tropical gateways? In *In proceedings of the Ocean Drilling Program: Scientific results* (Vol. 202, pp. 1–51).

Steph, S., Tiedemann, R., Prange, M., Groeneveld, J., Nürnberg, D., Reuning, L., et al. (2006). Changes in Caribbean surface hydrography during the Pliocene shoaling of the central American seaway. *Paleoceanography*, *21*(4). https://doi.org/10.1029/2004pa001092

Steph, S., Tiedemann, R., Prange, M., Groeneveld, J., Schulz, M., Timmermann, A., et al. (2010). Early Pliocene increase in thermohaline overturning: A precondition for the development of the modern equatorial pacific cold tongue. *Paleoceanography*, *25*(2). https://doi.org/10.1029/2008PA001645

Straub, M., Sigman, D. M., Ren, H., Martínez-García, A., Meckler, A. N., Hain, M. P., & Haug, G. H. (2013). Changes in North Atlantic nitrogen fixation controlled by ocean circulation. *Nature*, *501*(7466), 200–203. https://doi.org/10.1038/nature12397

Thirumalai, K., Quinn, T. M., & Marino, G. (2016). Constraining past seawater $\delta^{18}O$ and temperature records developed from foraminiferal geochemistry. *Paleoceanography*, *31*(10), 1409–1422.

Tiedemann, R., Sturm, A., Steph, S., Lund, S. P., & Stoner, J. (2007). Astronomically calibrated timescales from 6 to 2.5 Ma and benthic isotope stratigraphies, Sites 1236, 1237, 1239, and 1241. *Proceedings of the Ocean Drilling Program, Scientific Results*, *202*, 1–69.

Vallejo-Hincapié, F., Pardo-Trujillo, A., Barbosa-Espitia, Á., Aguirre, D., Celis, S. A., Giraldo-Villegas, C. A., et al. (2024). Miocene vanishing of the central American seaway between the Panamá arc and the South American plate. *Geological Society of America Bulletin*. https://doi.org/10.1130/B37499.1

Weigand, M. A., Foriel, J., Barnett, B., Oleynik, S., & Sigman, D. M. (2016). Updates to instrumentation and protocols for isotopic analysis of nitrate by the denitrifier method. *Rapid Communications in Mass Spectrometry*, *30*(12), 1365–1383. https://doi.org/10.1002/rcm.7570